Storage and Loss Characteristics of Coupled Poroviscoelastic and Hydrodynamic Systems for Biomimetic Applications

Patrick A. Smyth
Georgia Institute of Technology,
Department of Mechanical Engineering,
Atlanta, GA 30332
e-mail: pasmyth4@gatech.edu

Itzhak Green
Georgia Institute of Technology,
Department of Mechanical Engineering,
Atlanta, GA 30332
e-mail: itzhak.green@me.gatech.edu

Biotribology and biomechanics are evolving fields that draw from many disciplines. A natural relationship particularly exists between tribology and biology because many biological systems rely on tribophysics for adhesion, lubrication, and locomotion. This leads to many biomimetic inspirations and applications. The current study looks to mimic the function of articular cartilage in purely mechanical systems. To accomplish this goal, a novel coupling of phenomena is utilized. A flexible, porous, viscoelastic material is paired with a hydrodynamic load to assess the feasibility and benefit of a biomimetic thrust bearing. This study presents the dynamic properties of the coupled system, as determined from transient to steady operating states. The results indicate that bio-inspired bearings may have application in certain tribological systems, including biomechanical joint replacements, dampers, flexible rotordynamic bearings, and seals.
[DOI: 10.1115/1.4038958]

1 Introduction

The properties of articular cartilage make for an impressive tribological system. In healthy joints, articular cartilage is a phenomenal load bearing and wear resistant material [1,2]. There are many contributing mechanisms that make cartilage effective, with one important aspect being the coupled solid–fluid interactions of the collagen matrix and synovial fluid [3–9]. These coupled interactions make cartilage a desirable material to mimic outside of biological applications. The goal of the current study is to study cartilage-like materials operating in purely mechanical systems. The following study explores flexible/porous materials operating under hydrodynamic loads. The transient operation of the system is desired, as this is a proposed benefit of using a cartilage-like material in mechanical applications. Therefore, the coupled system is simulated in transient operation with a perturbation from steady-state. The results are compared to a traditional thrust bearing using the dynamic properties of storage and loss (defined herein).

A poroviscoelastic (PVE) model is proposed to mimic the function of cartilage. PVE materials are commonly used in cartilage modeling [7,10–13], and the two time-dependent mechanisms (permeability and viscoelasticity) give rich frequency domain characteristics (e.g., storage and loss). The PVE model is coupled to a hydrodynamic fluid load (HDL) with a modified Reynolds equation. The details of this coupling are found in a previous work [14]. The properties of storage and loss are assessed relative to a steady-state. These solutions indicate that the PVE/HDL combination is beneficial in certain tribological applications, particularly at relatively low frequencies (comparable to the gate of a human). Comparisons between the PVE/HDL model and a traditional HDL model are made with the correspondence principle, discussed in Sec. 2.

2 Background

The PVE/HDL problem is coupled with a combination of finite elements and finite difference/finite volume techniques. The details of this problem are presented in previous work [14]. The poroviscoelastic medium is a combination of viscoelastic solid grains and an imbibing Newtonian fluid (governed by Darcy's law). The fluid film is comprised of a Newtonian fluid for compatibility. The previous study simulated a coupled PVE/HDL thrust bearing to steady-state (equilibrium with a load, W), shown in Fig. 1 by the solid lines. Herein, dynamic properties of a similar system are obtained by perturbing the system from steady-state ($W + \Delta W$), shown in Fig. 1 by the dashed lines. The resulting properties of storage and loss give metrics that can be used to assess bearing dynamic performance across a frequency spectrum.

2.1 The Correspondence Principle and Mechanical Impedance. Following the techniques of Miller and Green [15,16] for gas film bearings, a correspondence principle is introduced for coupled PVE/HDL problems. The correspondence

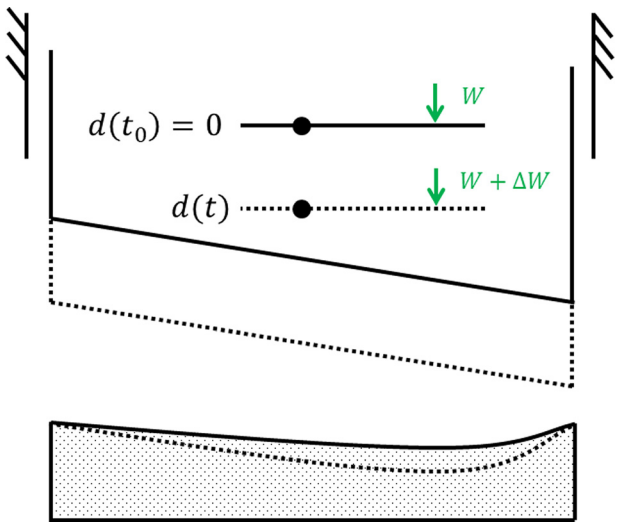

Fig. 1 Thrust bearing before and after load perturbation

Contributed by the Tribology Division of ASME for publication in the Journal of Tribology. Manuscript received October 17, 2017; final manuscript received December 17, 2017; published online February 9, 2018. Assoc. Editor: Min Zou.

principle follows the techniques used for viscoelastic materials. Retaining the convolution integral from linear viscoelasticity (i.e., Boltzmann's superposition principle [17]), a force–displacement relationship is proposed

$$F(t) = D(0)K(t) + \int_0^t \dot{D}(\gamma)K(t-\gamma)\,d\gamma \tag{1}$$

and

$$D(t) = F(0)C(t) + \int_0^t \dot{F}(\gamma)C(t-\gamma)\,d\gamma \tag{2}$$

In Eqs. (1) and (2), $F(t)$ is force, $D(t)$ is displacement, $K(t)$ is the stiffness modulus, and $C(t)$ is the compliance modulus. The stiffness and compliance moduli are analogous to the viscoelastic relaxation and creep moduli, respectively. Equations (1) and (2) are analogous to the stress–strain relationships given for linear viscoelasticity, where stress is translated to force, and strain to displacement.

2.2 Mechanical Impedance. A Laplace transform performed on Eqs. (1) and (2) provides a theoretical relationship between the stiffness and compliance moduli in the Laplace domain, forming the elastic-viscoelastic correspondence principle

$$F(s) = sK(s)D(s) \tag{3}$$

$$D(s) = sC(s)F(s) \tag{4}$$

Substituting Eq. (3) into Eq. (4) yields

$$sK(s) = \frac{1}{sC(s)} \tag{5}$$

Analogous to the complex modulus from viscoelasticity, $sK(s)$ is effectively a spring in the Laplace domain. Transferring from the Laplace domain to the frequency domain, $sK(s)$ has real and imaginary components

$$(i\omega)K(\omega) \triangleq K^*(\omega) = K'(\omega) + iK''(\omega) \tag{6}$$

The real part (K') is defined as the storage and the imaginary part (K'') as the loss. These properties are used to compare the PVE/HDL and rigid cases. For the current work, storage, and loss correspond to stiffness and damping, respectively, and are the critical metrics used to assess performance. In future work, other performance characteristics may be considered.

The physical significance of Eqs. (1)–(6) is that the storage and loss characteristics of a system are obtained with a single experiment, either by controlling load support or film thickness. This is done by imposing an instantaneous displacement in the film thickness and tracking the corresponding load support over time, or imposing an instantaneous change in load support and tracking the change in film thickness. The correspondence principle gives a mechanical impedance, from which storage and loss are found. This technique is advantageous because the combined poroviscoelastic behavior essentially behaves like a spring in the Laplace domain, making analysis straightforward. The relationship between the Laplace and frequency domains is also utilized in this work.

Previously, Miller and Green [15,16] imposed an instantaneous displacement on a gas film bearing to determine storage and loss. This method was consistent with a relaxation experiment and was supported because air is a compressible fluid (the equation of state allows for pressure calculations immediately after an instantaneous step at $t = t_0$). However, this is not possible in the HDL/PVE case, because the fluid and solid are considered incompressible. Therefore, an instantaneous displacement is impossible for the proposed cases (that are laterally constrained). This dictates that a relaxation experiment is not ideally suited to determine the storage and loss of the coupled PVE/HDL simulation (it is possible that a sufficiently fast, but finite, displacement may be imposed on the body in order to mimic relaxation). The alternative to relaxation is creep, which is physically possible in the current model. Here, a change in the load support is imposed, and the corresponding film thickness required to sustain this load is determined instantaneously. This technique is used in the current study to determine storage and loss.

2.3 Mechanical Impedance Models. As discussed earlier, to determine the mechanical impedance of the coupled PVE/HDL problem, a creep-like experiment is performed. First, the bearing in Fig. 1 is simulated to steady-state under a load, W. Then, from steady-state, the load is instantaneously perturbed and fixed ($W + \Delta W$), and the bearing's resulting travel is tracked. This creates a time-dependent force–displacement relationship. The force–displacement relationship is either translated into the frequency domain to determine storage and loss directly, or fit in the time domain with a constitutive model, whereby the fit parameters define the storage and loss. Using a known constitutive model is advantageous because it provides fit parameters that can be easily compared between configurations and simulations, and there are often direct correlations between the time domain fit and the frequency domain storage and loss moduli.

There is an analogous relationship between mechanical impedance and the complex modulus from viscoelasticity. Therefore, the spring-dashpot and fractional models used in viscoelasticity [14] can also model the force–displacement relationship. While the relaxation modulus is often considered in the definition of viscoelasticity, the mechanical impedance is determined from a creep-like test. An integer-order and fractional model are proposed as suitable models. The integer-order model is the well-known Kelvin–Voigt model, shown in Fig. 2(*a*). The fractional model emulates the Kelvin–Voigt model, replacing the dashpot with a fractional spring-pot of order α (Fig. 2(*b*)). The compliance of the Kelvin–Voigt model is [18]

$$C(t) = \frac{1}{K_{kv}}\left[1 - e^{-t/\tau}\right] \tag{7}$$

where the time constant, τ, relates the model parameters K_{kv} and η

$$\tau = \frac{\eta}{K_{kv}} \tag{8}$$

The compliance of the fractional Kelvin–Voigt model is [18]

$$C(t) = \frac{1}{K_f}\left\{1 - E_\alpha\left[-\left(\frac{t}{\nu}\right)^\alpha\right]\right\} \tag{9}$$

where E_α is the Mittag-Leffler function [19]

$$E_\alpha(z) = \sum_{k=0}^{\infty} \frac{z^k}{\Gamma(\alpha k + 1)} \tag{10}$$

In Eq. (10), z is an independent variable, and k is an index. ν relates the model parameters K_f and β

$$\nu = \frac{\beta}{K_f} \tag{11}$$

and takes the units of seconds (s). When $\alpha = 1$, the fractional calculus model reverts identically to the Kelvin–Voigt model, and when $\alpha = 1/2$, the complementary error function appears [2,14]. The integer-order and fractional models are capable of a creep-like behavior (fixed load with changing displacement), while

incapable of stress–relaxation-like behavior (instantaneous displacement is not possible). This mimics the physics of the coupled simulation with incompressible constituents. The models can be generalized by stacking additional elements in series [18]

$$C(t) = \sum_{n=0}^{\infty} \frac{1}{K_{f_n}} \left\{ 1 - E_{\alpha_n} \left[-\left(\frac{t}{\nu_n} \right)^{\alpha_n} \right] \right\} \tag{12}$$

The constitutive model for compliance, as given in Eq. (5), leads to storage and loss in the frequency domain

$$i\omega K(\omega) = K^*(\omega) = \frac{1}{i\omega C(\omega)} \tag{13}$$

Equation (12) is converted from the time domain to the Laplace domain

$$C(s) = \sum_{n=0}^{\infty} \frac{1}{K_{f_n}} \left(\frac{1}{s} - \frac{1}{s(1 + a_n s^{\alpha_n})} \right) \tag{14}$$

with

$$a_n = \left(\frac{1}{\nu_n} \right)^{\alpha_n} \tag{15}$$

Multiplying the two sides of Eq. (14) by "s" gives

$$sC(s) = \sum_{n=0}^{\infty} \frac{1}{K_{f_n}} \left[1 - \frac{1}{(1 + a_n s^{\alpha_n})} \right] \tag{16}$$

From Eqs. (5), (6), and (13), the storage and loss properties of the coupled PVE/HDL system are expediently obtained from the compliance data. The physics of the integer and fractional Kelvin–Voigt models suggests that the storage and loss values trend to infinity at high frequencies. This is consistent with the coupled HDL/PVE problem, in that an instantaneous displacement ($\omega \rightarrow \infty$) is not possible in the system. If compressibility is allowed, or the solid is not confined as described earlier (i.e., an instantaneous deformation is possible at $t = 0$), the storage and loss values will be finite as $t = 0$ or $\omega \rightarrow \infty$.

Compared to the rigid case, the flexible interface of the poroviscoelastic pad poses a unique challenge in the description of the film profile because of deformation. In the rigid case, the film profile can be determined by knowing the initial geometry and one point along the bearing's interface. For the flexible case, it is not sufficient to know the coordinates of a single point on the pad, as the deformation of the entire porous pad dictates the film thickness. Therefore, some ambiguity exists in describing the time history of the film thickness. For the purposes of the current work, the bearing's location at steady-state serves as "zero" (see Fig. 1). A point on the bearing is chosen as the tracking point, and all displacements are measured relative to this position. The displacement, $D(t)$, is the magnitude of the bearing's response from steady-state

$$D(t) = |d(t) - d(t_0)| \tag{17}$$

Letting steady-state be defined as $d(t_0) = 0$, then

$$D(t) = |d(t)| \tag{18}$$

This definition of displacement is a "triboelement centric" view of the system dynamics, and it serves as a platform for comparing the different cases. The aforementioned models are fit to the displacement time history when subjected to a set load perturbation. From the fit, analytical expressions exist to determine the mechanical impedance in the Laplace domain, leading to the properties of storage and loss in the frequency domain. In the foregoing work, the results are obtained from the numerical procedure described in Ref. [14], where the porous Reynolds equation is coupled to the structural poroviscoelasticity by ABAQUS and associated subroutines.

3 Results

A number of cases are explored herein to understand the dynamic effects of the permeable and viscoelastic contributions. Table 1 gives the relevant simulation parameters used to determine steady-state. Numerous permeability values in the neighborhood of articular cartilage ($k \approx 10^{-16}$ m^2) are explored. The transient response of the coupled PVE/HDL problem is obtained by perturbing the load support. This occurs from steady-state and is equivalent to a weight being added to the bearing at time $t = t_0$. The results of the simulations to steady-state are given in Ref. [20]. In the transient case, the magnitude of the fluid film's response is tracked in time, as shown in Fig. 3. The information in Fig. 3 gives displacement of the bearing versus time for a known incremental load ($\Delta W = 12$ N/m). The compliance modulus is fit to these data. With the compliance modulus, the dynamic properties of storage and loss are obtained, as outlined earlier.

Herein, the terminologies "rigid," "flexible," "nonporous," and "porous" are used to describe the mechanism(s) apparent in the substrate. Rigid means that the bearing surface does not deform, while flexible means that the surface can deform. Nonporous, or impermeable, means that no fluid can flow vertically across the bearing surface, and porous means that fluid can flow in the vertical direction.

3.1 Rigid and Impermeable Case. The rigid and impermeable case is common in tribological applications and is given as a benchmark example. The displacement path (i.e., Fig. 3) is fit with the fractional calculus Kelvin–Voigt model, shown in Fig. 4(*a*). The fit parameters are given in Table 2, and the

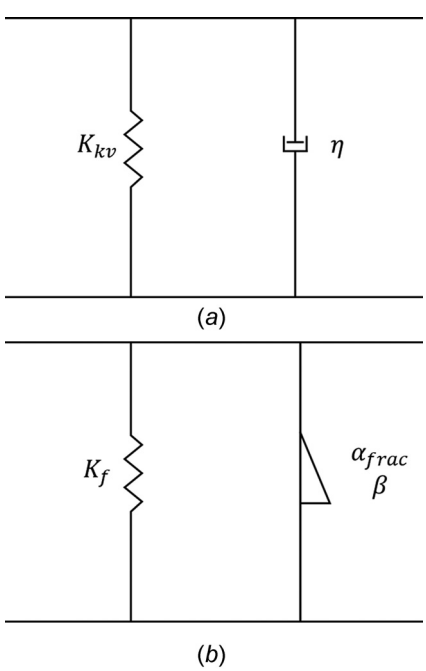

Fig. 2 Mechanical analogy for the compliance models used to determine force/displacement relationship: (*a*) Kelvin–Voigt viscoelastic model and (*b*) fractional representation of the Kelvin–Voigt viscoelastic model

Table 1 Geometric parameters for PVE/HDL analysis

Parameter	Symbol	Value (units)
Load per depth	W	600 (N/m)
PVE pad length	L	25 (mm)
PVE pad height	H	6.25 (mm)
Bearing velocity	U_1	0.02 (m/s)
Fluid viscosity	μ	0.1 (Pa·s)
Slip coefficient	α	0.1
Initial inlet film thickness	h_i	40 (μm)
Film thickness ratio	a	2.2

frequency-dependent storage and loss properties are shown in Fig. 4(*b*). For the rigid, impermeable cases, the fractional derivative is nearly one ($\alpha \approx 1$), which indicates that the fractional element is essentially a damper and the model is nearly the traditional Kelvin–Voigt model. In this case, the storage is virtually constant, and the loss is virtually linear. The dynamic property of damping is defined as the loss modulus divided by frequency

$$B(\omega) = \frac{K''(\omega)}{\omega} \tag{19}$$

The damping in the rigid/impermeable case is practically constant. This translates to constant stiffness and damping, exactly like a spring and dashpot in parallel. These results are consistent with a purely viscous response.

3.2 Rigid and Permeable Cases. The effect of permeability on storage and loss is studied in the rigid case (no material deformation). The permeability is varied from the impermeable case to a value of $k = 10^{-13}$ m^2. Increasing the permeability beyond this point is not suitable for the example parameters given (the bearing cannot support the load requirements). Under the same perturbation load ($\Delta W = 12$ N/m), the compliance results are shown in Fig. 5 for various permeabilities. The results given in Table 2 show that the K term decreases with an increase in permeability, while ν increases with permeability. However, the character of the storage and loss is relatively unchanged by the permeability. This is indicated by the fractional derivative value not changing significantly from the impermeable to the most permeable cases ($\alpha \approx 1$). Therefore, the storage properties of the system stay nearly constant with frequency, and the loss properties are practically linear with frequency, similar to that shown in Fig. 4(*b*).

In the permeable region where triboelement operation is possible ($k \lesssim 10^{-13}$ m^2), the effect of permeability alone is not significant enough to change the storage and loss character (α remains approximately 1). This is indicated in Table 2 and Figs. 4(*b*) and 5, where the response is shown to effectively be a spring and damper in parallel. However, the mechanism of permeability is still influential in the bearing's performance, as the storage decreases with an increase in permeability, and the loss increases

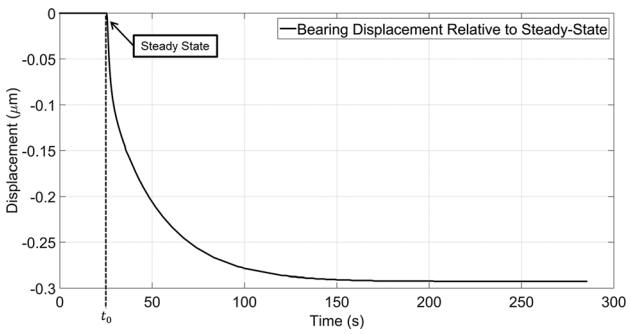

Fig. 3 Change in bearing height due to a 2% ($\Delta W = 12$ N/m) load perturbation

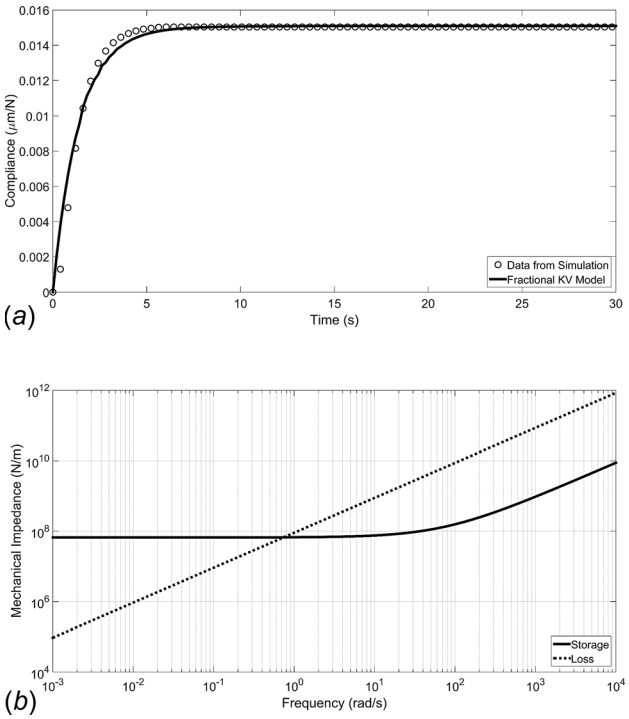

Fig. 4 Compliance, storage and loss in the rigid/nonporous case: (*a*) compliance in the rigid/nonporous case, with fit given in Table 2 and (*b*) storage and loss in the rigid/nonporous case

Table 2 Storage and loss fit to simulation data (rigid configuration)

k (m^2)	K_f (N/m)	ν (s)	α	h_o (μm)
Nonporous	6.64×10^7	1.363	0.991	18.1
10^{-16}	6.67×10^7	1.363	0.993	18.0
10^{-15}	6.67×10^7	1.363	0.993	17.8
10^{-14}	6.49×10^7	1.365	0.993	16.9
10^{-13}	4.93×10^7	1.888	0.988	12.1

with increasing permeability. Discussed herein, the combination of permeability and flexibility gives rich frequency-dependent behavior. This is because permeability changes the action of deformation in the porous pad. In likelihood, the permeability does change the storage and loss characteristics significantly, but this occurs outside of the operational region for the considered case.

3.3 Flexible (PVE) Cases. The performance of triboelements with flexible–porous interfaces is explored using a thrust bearing, like that of Fig. 1, in a "long bearing" configuration

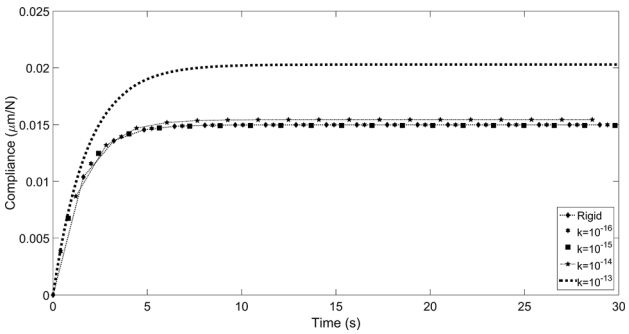

Fig. 5 Compliance in the rigid/porous cases

(corresponding to plane strain in the poromechanics). The geometry and specifications of the problem are given in Table 1. The PVE pad is "glued" at the lateral edges ($x=0$ and $x=L$) of the PVE pad. In this application, glued means that the PVE pad is fixed at the edges, and no strain occurs at the boundary. However, fluid is still allowed to permeate across the porous boundary. Figure 6 shows the boundary conditions imposed on the porous pad. Assuming a submerged bearing, the leading and trailing edges of the pad are exposed to atmospheric pressure (gauge), which allows fluid flow across the boundary. The bottom boundary is fixed and rigid, and the top boundary is flexible and the pressure, p, is equal to the fluid film pressure, P. The pressure gradient in the porous pad facilitates fluid flow throughout the pad. The pressure boundary and initial conditions are defined mathematically

$$p(0,y,t) = p(L,y,t) = 0 \tag{20}$$

$$\frac{\partial p}{\partial y}(x,-H,t) = 0 \tag{21}$$

$$p(x,0,t) = P(x,0,t) \tag{22}$$

$$p(x,y,0) = 0 \tag{23}$$

$$\varepsilon_x(0,y,t) = \varepsilon_x(L,y,t) = 0 \tag{24}$$

$$\varepsilon_y(0,y,t) = \varepsilon_y(L,y,t) = 0 \tag{25}$$

$$\varepsilon_x(x,-H,t) = \varepsilon_y(x,-H,t) = 0 \tag{26}$$

$$\sigma_x(x,0,t) = 0 \tag{27}$$

$$\sigma_y(x,0,t) = -P(x,0,t) \tag{28}$$

$$\sigma_x(x,y,0) = \sigma_y(x,y,0) = 0 \tag{29}$$

Equations (20)–(22) enforce the fluid pressure boundary conditions, while Eqs. (24)–(28) are placed on the biomimetic solid matrix. Equation (21) enforces no flow across the rigid boundary at $y=-H$. Figure 6(*a*) shows the boundaries where flow exists,

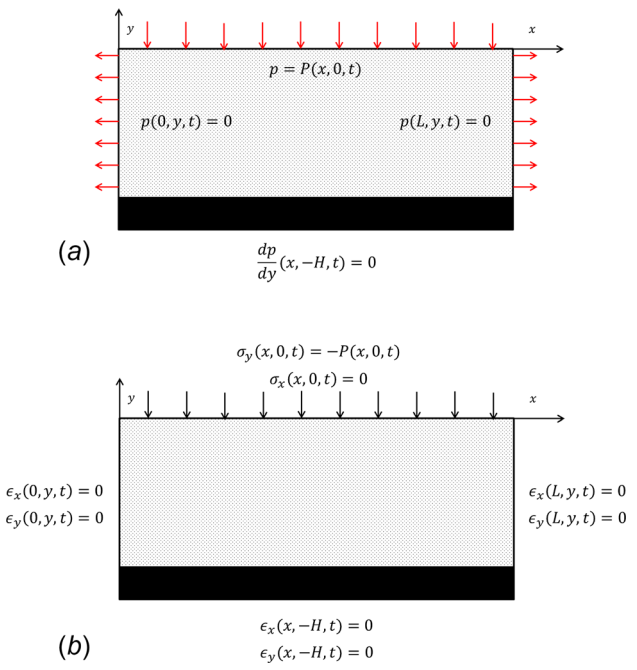

Fig. 6 Fluid and solid boundary conditions on porous pad (case I): (*a*) fluid pressure boundary conditions on the PVE pad and (*b*) solid boundary conditions on the PVE pad

and these values are determined from the fluid pressure gradients. Pressure boundary conditions are enforced to maintain continuity with the HDL solution from the Reynolds equation [20]. Initial conditions in Eqs. (23) and (29) provide the undisturbed loading conditions at time $t=0$.

The boundary conditions in Fig. 6 are used to compare the rigid/nonporous case to the flexible PVE cases. This fixes the PVE pad at the lateral edges but still allows for deformation in the PVE body due to fluid exodus. The boundary conditions provide the best platform for comparison purposes with the rigid cases. The flexible/porous case has two additional material mechanisms compared to the rigid case: permeability and viscoelasticity. A representative set of viscoelastic parameters is used in ABAQUS (Table 3). These parameters are derived from previous study of articular cartilage [1].

Figure 7(*a*) shows the compliance of the flexible/nonporous and rigid/nonporous cases. Two important differences exist between the flexible/nonporous and rigid/nonporous cases: (1) the flexible/nonporous case has significantly more compliance than the rigid/nonporous case and (2) the flexible/nonporous case cannot be fit with a single fractional order model. Rather, a two element chain of fractional Kelvin–Voigt elements is required (Fig. 8). The implications of this are significant because it shows the impact of the viscoelastic/permeable component.

Figure 7(*b*) shows the dynamic storage and loss of the rigid/nonporous and flexible/nonporous cases. The flexible/nonporous case shows that the viscoelastic action manifests in the storage and loss results. The flexible/nonporous case has a higher loss across the frequency spectrum versus the rigid/nonporous case. At low frequencies, the flexible/nonporous case has lower storage than its rigid/nonporous counterpart. However, as the frequency increases, the storage in the flexible/nonporous case increases beyond the rigid/nonporous case. This is due to the frequency-dependent portions of the fractional spring-pots that are associated with the storage modulus. The viscoelastic case has a larger component attributed to the frequency-dependent storage modulus (i.e., $\alpha_n < 1$) than the rigid case. Physically, this increase in storage is attributed to the reduced film thickness in the flexible cases (Fig. 9(*a*)). Tables 2 and 3 indicate that the flexible cases generally have smaller film thicknesses than their rigid counterparts. This is also shown in the pressure profiles, given in Fig. 9(*b*). The load support (area under the curve) is identical between rigid/nonporous and flexible/porous cases, but the shape and load center is different to accommodate the deformation and flow in the flexible/porous case. The smaller film thickness generates higher storage values, but viscoelasticity also influences the storage properties. Therefore, the total response is a combination of these effects. Viscoelasticity also changes the character of the response. This differentiates the rigid and flexible cases, and

Table 3 ABAQUS inputs for viscoelastic component

Parameter	Symbol	Value (units)
Poisson's ratio (instantaneous)	ν	0.3
Elastic modulus (instantaneous)	E	15.0 (MPa)
Perturbation	ΔW	(0.02) W
Prony constant (bulk)	k_1	0.152
	k_2	0.135
	k_3	0.310
	k_4	0.217
Prony constant (shear)	g_1	0.152
	g_2	0.135
	g_3	0.310
	g_4	0.217
Prony time constant	τ_1	7.682 (s)
	τ_2	0.238 (s)
	τ_3	2.229 (s)
	τ_4	5.617 (s)

means that there is a region of the frequency response that may be tunable by controlling the viscoelastic and/or permeable action. The impact of permeability when the viscoelastic mechanism is included is explored next.

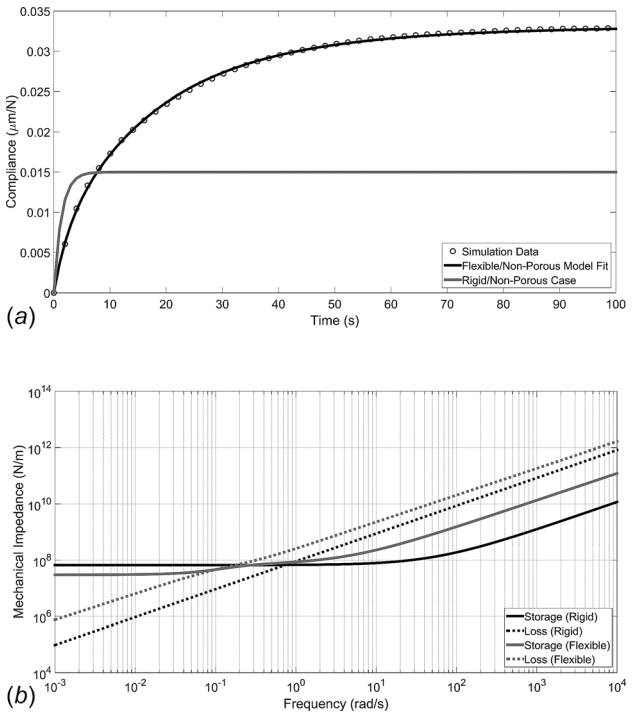

Fig. 7 Compliance, storage and loss in the rigid/nonporous and flexible/nonporous cases: (*a*) compliance in the rigid/nonporous case versus the flexible/nonporous case and (*b*) storage and loss in the rigid/nonporous case versus the flexible/nonporous case

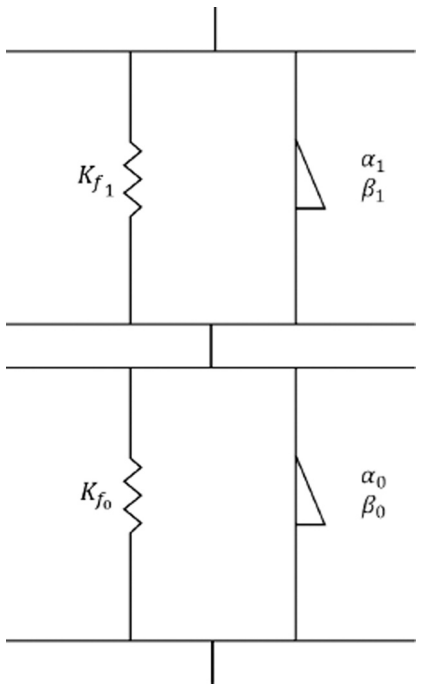

Fig. 8 Two element chain of fractional Kelvin–Voigt elements

An example of the flexible and porous case is shown in Fig. 10. Here, the viscoelastic and porous actions occur simultaneously. The fit parameters in Table 3 indicate what is happening in Fig. 10. In the flexible/porous cases, the fractional derivatives, α_n, deviate dramatically from the rigid/nonporous and flexible/nonporous cases, where $\alpha \approx 1$. As α approaches 1/2, the viscoelastic response is clearly seen. Figure 10 shows this clear viscoelastic response at low frequencies, followed by a viscously dominated response at higher frequencies. Combining permeability and viscoelasticity changes the character of the response appreciably from the rigid/nonporous case and flexible/nonporous cases. The combined permeability and viscoelasticity play a governing role in the storage and loss characteristics. Essentially, the time scale of the path that the triboelement takes after a perturbation is changed, and the resulting storage and loss character is altered. Without the viscoelastic action, the permeability has a relatively small effect on the triboelement's dynamic performance; however, with the coupled viscoelasticity, the dynamic performance is significantly altered. This is apparent in the fit parameters given in Table 4, where the K, ν, and α values are tangibly different for the flexible/porous and flexible/nonporous cases.

3.4 Tunable Dynamic Performance. It has been shown that the dynamic performance of a triboelement is changed with the introduction of a porous substrate. From a design standpoint, a number of degrees-of-freedom exist in the triboelement characteristics. These include geometric changes in the bearing (inclination, etc.) and in the porous pad (pad length, depth, etc.), as well as material changes (permeability, viscoelastic properties, etc.).

The HDL/PVE system has two important mechanisms that influence the storage and loss: the permeability and the viscoelastic action. In particular, as the permeability drops in the coupled HDL/PVE system, the viscoelastic flexibility in the porous pad still acts to change the dynamic properties of the triboelement. Having two mechanisms that influence the dynamic

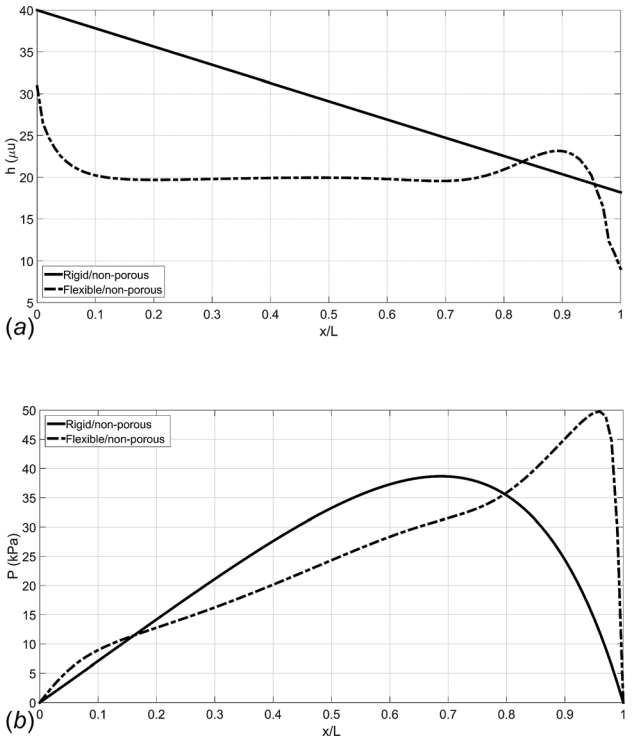

Fig. 9 Final steady-state results of rigid/nonporous and flexible/nonporous solutions: (*a*) film thicknesses of the rigid/nonporous and flexible/nonporous cases and (*b*) pressure profiles of the rigid/nonporous and flexible/nonporous cases

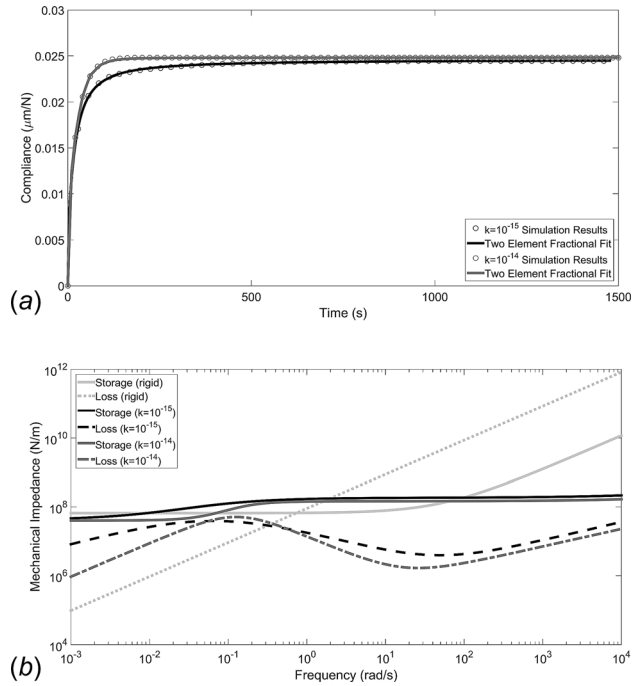

Fig. 10 Compliance, storage and loss in the flexible/porous cases: (*a*) compliance in the flexible/porous cases and (*b*) storage and loss in the flexible/porous cases

storage and loss gives a great deal of flexibility in triboelement design.

The takeaway of this analysis is that there exists a tradeoff between the storage and loss properties of a flexible/porous bearing. The porous cases presented are able to sustain loads comparable to the rigid case. Therefore, the penalty of using a flexible/porous bearing is likely not prohibitive. Loss is increased in the flexible/porous triboelements. In certain applications, this is a preferable operating condition. Some additional benefits are hypothesized too. These include the following: lubricant availability in the porous pad if a loss of lubricant occurs, increased ability to mitigate shock events, and potential operation in a full film regime for longer compared to the rigid case.

3.5 Region of Applicability. The storage and loss results given herein are determined from a 2% load perturbation. In the small region around the operating load, the results are assumed linear with the load perturbation. Therefore, the perturbation magnitude does not influence the storage and loss results. In limited testing, this assumption has proven to be correct, and the load perturbation has been tested up to approximately 5% before the simulation fails to converge.

The simulations presented herein are stable across a spectrum of frequencies. In other words, the PVE/HDL concept did not introduce instabilities in an otherwise stable thrust bearing. Clearly, any system must be designed to be stable. For example, in rotordynamic systems, "internal damping" is known to instigate dynamic instabilities [21,22]. That is, systems should possess positive-definite stiffness, and the eigenvalues must contain decaying real parts [21,22]. This study does not replace that need for any general tribo-system.

Table 4 Storage and loss fit to simulation data

k (m^2)	K_{f_n} (N/m)	ν_n (s)	α_n	h_o (μm)
Flexible/nonporous	1.59×10^8	2.568	0.968	9.06
	3.68×10^8	23.764	0.934	
10^{-15}	1.86×10^8	8.32×10^{-6}	0.5367	6.01
	5.19×10^7	176.93	0.6278	
10^{-14}	1.46×10^8	5.17×10^{-6}	0.5125	5.08
	5.56×10^7	29.60	0.9779	

4 Discussion

The Reynolds equation (see Ref. [20]) is modified from the rigid case to describe the fluid mechanics of a thin film interacting with a porous substrate. Permeability is shown to have a strong coupling effect on the porous Reynolds equation. In order to simulate the transient behavior of the PVE/HDL system, continuously updating numerical schemes are required.

The results presented here are promising in a number of ways. First, the simulations prove that a coupled PVE/HDL problem is feasible in a tribological sense. Specifically, a porous/flexible pad can sustain a load that is comparable to its rigid counterpart [14]. However, the load support of the triboelement is strongly influenced by the permeability of the porous pad [14,23,24]. Ideally, a tradeoff exists between permeability and the dynamic properties of interest. In the rigid/porous cases, Fig. 5 indicates that the compliance changes with respect to permeability. This has the effect of changing the storage and loss values for the triboelement. However, the character of the storage and loss (i.e., the frequency-dependent shape) is relatively unchanged by the permeability. This is noted by the fit value α remaining nearly 1, meaning that the fractional spring-pot is a simple viscous damper. This indicates that permeability alone will not give the designer a great deal of control over the dynamic properties of the triboelement. A flexible interface is considered for this purpose.

Figure 7 compares the compliance of a rigid/nonporous and flexible/nonporous design. The viscoelastic action changes the compliance relative to the viscous action of the rigid case. In the flexible case, there exists a coupled response that is partially viscous (from the fluid) and partially viscoelastic (from the pad). A second modeling element (fractional Kelvin–Voigt) is required to adequately capture this response. The flexible case displays additional loss in the frequency domain compared to the rigid/nonporous case. This is due to the secondary dissipation mechanism of the porous pad. However, the character of the loss modulus is essentially unchanged, while the storage modulus picks up a frequency-dependent component from the complex stiffness modulus. The real component of the fractional spring-pot element contributes to the storage modulus and is multiplied by ω, which explains its trend as ω grows.

When the flexible and permeable cases are combined, the dynamic properties take a new shape relative to the previously discussed cases. Figure 10(*b*) shows the effect of the coupled dissipation mechanisms, particularly when those mechanisms have different time-scales. Here, there appears to be an element of user control, or tunability, in the dynamic properties. This can be seen between the permeability cases k^{-14} and k^{-15}. The application of the loss modulus, which is related to damping, could be tuned to mitigate vibrations in a particular band of frequencies. This is one goal of the current study, and the results indicate that there is promise in the unique coupling of PVE/HDL.

The "big-picture" view of this work is that it proves the feasibility of a coupled flexible/porous material with a hydrodynamic fluid load. Not only can bearing designs of this nature support tribological loads, the material properties can be manipulated to change the dynamic storage and loss characteristics. The importance of this should not be understated. The current work provides both insight into how certain natural systems work, and also a toolbox for exploring tribological applications. More complicated porous mediums and fluid mechanics can be extended from this work.

5 Conclusions

The genesis of coupled PVE/HDL comes from biomimetics, where biological solutions exist for many tribological problems.

With biological materials, the engineer cannot control the material properties; however, the physics can be described. The proposed PVE/HDL model describes the physics of a flexible/porous material interacting with a fluid film load. Potentially, the model has use in the study of biological mechanisms, as well as biomimetic tribological applications. Articular cartilage is of particular interest in biomimetics because of its adaptability and longevity. Coupling mechanisms like a fluid film and porous pad helps to translate from biomechanical to tribological applications.

New demands in triboelement performance require innovative technology. A coupled HDL/PVE bearing is a feasible configuration for certain applications. These include biomechanics, flexible bearing technology, and sealing elements. In addition, PVE materials have strong dissipation characteristics, making them suitable for shock absorption and damping elements. The results of the coupled HDL/PVE simulation indicate that flexible, porous substrates can promote tunable triboelement performance. While the current work shows improved loss at low frequencies, different material combinations could give more dissipation at other frequency spectra (e.g., frequencies experienced in rotating machinery). This can potentially improve tribological considerations, especially wear and damping. However, there are tradeoffs associated with these gains, namely, with film thicknesses and storage values at certain frequencies. Additional study is required to quantify this performance and make comparisons between conventional and bio-inspired systems.

Nomenclature

a = film inlet to outlet ratio (h_i/h_o)
B = dynamic damping
C = compliance modulus
D = displacement
F = force
h = fluid film thickness
h_i = inlet fluid film thickness
h_o = outlet fluid film thickness
H = bearing pad height
k = permeability
K = stiffness modulus
K_f = fractional spring constant
K_{kv} = Kelvin–Voigt spring constant
K' = storage modulus
K'' = loss modulus
L = bearing pad length
t = time
U_1 = bearing velocity
α = fractional derivative
β = spring-pot constant
γ = dummy variable
ε_{ij} = strain
η = dashpot constant
μ = lubricant viscosity
ν = fractional time constant
σ_{ij} = stress
τ = time constant
ω = frequency

References

[1] Smyth, P. A., Green, I., Jackson, R. L., and Hanson, R. R., 2014, "Biomimetic Model of Articular Cartilage Based on In Vivo Experiments," J. Biomimetics, Biomaterials Biomed. Eng., **21**, pp. 75–91.
[2] Smyth, P. A., and Green, I., 2015, "Fractional Calculus Model of Articular Cartilage Based on Experimental Stress-Relaxation," Mech. Time-Dependent Mater., **19**(2), pp. 209–228.
[3] Mow, V., Gu, W., and Chen, F., 2005, "Structure and Function of Articular Cartilage and Meniscus," *Basic Orthopaedic Biomechanics & Mechano-Biology*, 3rd ed., Lippincott Williams & Wilkins, Philadelphia, PA, pp. 181–258.
[4] Mow, V. C., Kuei, S. C., Lai, W. M., and Armstrong, C. G., 1980, "Biphasic Creep and Stress Relaxation of Articular Cartilage in Compression: Theory and Experiments," ASME J. Biomech. Eng., **102**(1), pp. 73–84.
[5] Mak, A. F., 1986, "The Apparent Viscoelastic Behavior of Articular Cartilage—The Contributions From the Intrinsic Matrix Viscoelasticity and Interstitial Fluid Flows," ASME J. Biomech. Eng., **108**(2), pp. 123–130.
[6] Suh, J. K., and DiSilvestro, M. R., 1999, "Biphasic Poroviscoelastic Behavior of Hydrated Biological Soft Tissue," ASME J. Appl. Mech., **66**(2), pp. 528–535.
[7] Setton, L. A., Zhu, W., and Mow, V. C., 1993, "The Biphasic Poroviscoelastic Behavior of Articular Cartilage: Role of the Surface Zone in Governing the Compressive Behavior," J. Biomech., **26**(4–5), pp. 581–592.
[8] Ateshian, G. A., Wang, H., and Lai, W. M., 1998, "The Role of Interstitial Fluid Pressurization and Surface Porosities on the Boundary Friction of Articular Cartilage," ASME J. Tribol., **120**(2), pp. 241–248.
[9] Ateshian, G. A., 2009, "The Role of Interstitial Fluid Pressurization in Articular Cartilage Lubrication," J. Biomech., **42**(9), pp. 1163–1176.
[10] Wilson, W., van Donkelaar, C. C., van Rietbergen, B., Ito, K., and Huiskes, R., 2004, "Stresses in the Local Collagen Network of Articular Cartilage: A Poroviscoelastic Fibril-Reinforced Finite Element Study," J. Biomech., **37**(3), pp. 357–366.
[11] Wilson, W., van Donkelaar, C. C., van Rietbergen, B., and Huiskes, R., 2005, "A Fibril-Reinforced Poroviscoelastic Swelling Model for Articular Cartilage," J. Biomech., **38**(6), pp. 1195–1204.
[12] DiSilvestro, M. R., Zhu, Q., and Suh, J.-K. F., 2001, "Biphasic Poroviscoelastic Simulation of the Unconfined Compression of Articular Cartilage—II: Effect of Variable Strain Rates," ASME J. Biomech. Eng., **123**(2), pp. 198–200.
[13] DiSilvestro, M. R., and Suh, J.-K. F., 2001, "A Cross-Validation of the Biphasic Poroviscoelastic Model of Articular Cartilage in Unconfined Compression, Indentation, and Confined Compression," J. Biomech., **34**(4), pp. 519–525.
[14] Smyth, P. A., and Green, I., 2017, "Analysis of Coupled Poroviscoelasticity and Hydrodynamic Lubrication," Tribol. Lett., **65**(1), pp. 1–10.
[15] Miller, B., and Green, I., 1998, "Constitutive Equations and the Correspondence Principle for the Dynamics of Gas Lubricated Triboelements," ASME J. Tribol., **120**(2), pp. 345–352.
[16] Miller, B., and Green, I., 2001, "Numerical Formulation for the Dynamic Analysis of Spiral-Grooved Gas Face Seals," ASME J. Tribol., **123**(2), pp. 395–403.
[17] Gurtin, M. E., and Sternberg, E., 1962, "On the Linear Theory of Viscoelasticity," Archive Rational Mech. Anal., **11**(1), pp. 291–356.
[18] Koeller, R., 1984, "Applications of Fractional Calculus to the Theory of Viscoelasticity," ASME J. Appl. Mech., **51**(2), pp. 299–307.
[19] Erdélyi, A., Magnus, W., Oberhettinger, F., and Tricomi, F. G., eds., 1955, *Higher Transcendental Functions*, Vol. III, McGraw-Hill, New York.
[20] Smyth, P. A., Varney, P. A., and Green, I., 2016, "A Fractional Calculus Model of Viscoelastic Stator Supports Coupled With Elastic Rotor–Stator Rub," ASME J. Tribol., **138**(4), p. 041101.
[21] Green, I., 1990, "Gyroscopic and Damping Effects on the Stability of a Noncontacting Flexibly-Mounted Rotor Mechanical Face Seal," Dyn. Rotating Mach., pp. 153–173.
[22] Miller, B., and Green, I., 1997, "On the Stability of Gas Lubricated Triboelements Using the Step Jump Method," ASME J. Tribol., **119**(1), pp. 193–199.
[23] Prakash, J., and Vij, S., 1974, "Analysis of Narrow Porous Journal Bearing Using Beavers-Joseph Criterion of Velocity Slip," ASME J. Appl. Mech., **41**(2), pp. 348–354.
[24] Etsion, I., and Michael, O., 1994, "Enhancing Sealing and Dynamic Performance With Partially Porous Mechanical Face Seals," Tribol. Trans., **37**(4), pp. 701–710.